Journal of Biomedical Optics

SPIEDigitalLibrary.org/jbo

Multimodal tissue imaging: using coregistered optical tomography data to estimate tissue autofluorescence intensity change due to scattering and absorption by neoplastic epithelial cells

Hamid Pahlevaninezhad
Ivana Cecic
Anthony M. D. Lee
Alastair H. Kyle
Stephen Lam
Calum MacAulay
Pierre M. Lane

Multimodal tissue imaging: using coregistered optical tomography data to estimate tissue autofluorescence intensity change due to scattering and absorption by neoplastic epithelial cells

Hamid Pahlevaninezhad, Ivana Cecic, Anthony M. D. Lee, Alastair H. Kyle, Stephen Lam, Calum MacAulay, and Pierre M. Lane
BC Cancer Agency, 675 West 10th Avenue, Vancouver, British Columbia, V5Z 1L3 Canada

Abstract. Autofluorescence (AF) imaging provides valuable information about the structural and chemical states of tissue that can be used for early cancer detection. Optical scattering and absorption of excitation and emission light by the epithelium can significantly affect observed tissue AF intensity. Determining the effect of epithelial attenuation on the AF intensity could lead to a more accurate interpretation of AF intensity. We propose to use optical coherence tomography coregistered with AF imaging to characterize the AF attenuation due to the epithelium. We present imaging results from three vital tissue models, each consisting of a three-dimensional tissue culture grown from one of three epithelial cell lines (HCT116, OVCAR8, and MCF7) and immobilized on a fluorescence substrate. The AF loss profiles in the tissue layer show two different regimes, each approximately linearly decreasing with thickness. For thin cell cultures (<300 μm), the AF signal changes as $AF(t)/AF(0) = 1 - 1.3t$ (t is the thickness in millimeter). For thick cell cultures (>400 μm), the AF loss profiles have different intercepts but similar slopes. The data presented here can be used to estimate AF loss due to a change in the epithelial layer thickness and potentially to reduce AF bronchoscopy false positives due to inflammation and non-neoplastic epithelial thickening. [DOI: 10.1117/1.JBO.18.10.106007]

Keywords: lung cancer; autofluorescence bronchoscopy; optical coherence tomography; optical scattering; three-dimensional cell cultures; histology; epithelium; stroma.

Paper 130435RR received Jun. 24, 2013; revised manuscript received Sep. 11, 2013; accepted for publication Sep. 19, 2013; published online Oct. 9, 2013.

1 Introduction

Lung cancer is the leading cause of cancer death worldwide.[1] Techniques for early detection of lesions in the intraepithelial (preinvasive) stage are extremely important, as they lead to better patient outcomes. Intraepithelial neoplastic lesions, however, are difficult to detect by conventional white-light bronchoscopy, as the changes associated with these lesions are very subtle under white-light illumination.

Autofluorescence (AF) bronchoscopy is an established clinical technique that uses blue light to excite natural tissue fluorescence in the airways. This imaging technique has proven to be extremely effective for the early detection of lung cancer by aiding in the identification of abnormal areas from which biopsies should be collected.[2,3] AF bronchoscopy detects the lesion with up to 6× more sensitivity. Normal tissue emits pale-green native tissue fluorescence when illuminated with blue light (410 to 460 nm) due to elastin and collagen contents in the submucosa. The increased number of cells with larger nuclear-to-cytoplasmic ratios, more active metabolic state, and increased blood content associated with abnormal tissue result in the emission of markedly dimmer green AF with increased relative red AF emission. However, the improved sensitivity of AF bronchoscopy for the detection of pre-neoplastic lesions comes at the cost of a decreased specificity. Epithelium of early lung cancers has structural characteristics (cellular density, nuclear structure, and thickness) which differ from that of normal tissue. However, some non-neoplastic conditions can mimic some of the characteristics of early cancers. For instance, thickening of epithelium due to inflammation or trauma does not necessarily correlate with cancer, but it does reduce the AF signal due to increased scattering and structural changes in the submucosa, leading to false positives. As a result, AF bronchoscopy suffers from a rather high false-positive rate (about 40%).

Optical scattering and absorption of the epithelium layer alter the AF signal intensity originating from stroma. Modeling the effect of AF scattering and absorption may help achieve more accurate interpretation of AF intensity. The optical scattering of tissue has been the subject of intense research.[4–9] In particular, several techniques are available for AF intensity correction in the literature including empirical techniques, measurement-based techniques, and theory-based techniques. A comprehensive review of these methods can be found in Ref. 10. In the empirical techniques, a ratio of fluorescence to reflectance at one or two excitation wavelengths is utilized to correct for change in fluorescence due to blood content.[11–15] This technique is based on Jöbsis et al.'s postulate, which assumes blood vessels totally absorb both excitation and emission light.[11] However, Sterenborg et al. showed that the method was not an effective correction technique due to a significant correlation between the ratio and skin color.[16] Measurement-based techniques rely on selectively recording AF photons that travel a short distance

Address all correspondence to: H. Pahlevaninezhad, BC Cancer Agency, 675 West 10th Avenue, Vancouver, British Columbia, Canada V5Z 1L3. Tel: 604-676-8082; Fax: 604-675-8099; E-mail: hpahleva@bccrc.ca

through tissue and, therefore, are distorted the least by scattering and absorption. An example is the confocal technique[17] that has been confirmed to be effective in reducing scattering distortions by experimental work and Monte Carlo modeling.[18–20] Biswal et al. proposed using polarized light to selectively measure photons that, on average, undergo less scattering using the fact that polarization information is lost during the scattering process.[21] However, techniques of this sort work for rather shallow depths of tissue compared with the standard measurement techniques. The theoretical methods are mainly based on the modified Beer–Lambert law, the Kubelka–Munk theory, and diffusion theory.[10,22–27] Most of these theoretical techniques assume that the optical properties of the tissue are uniform, leading to less accurate results.[27,28]

Optical coherence tomography (OCT) is an interferometric technique for obtaining sub-surface images of biological tissue and providing images with less than 10-μm axial resolution and >1-mm penetration depth.[29–31] OCT employs nonionizing, near-infrared radiation to capture real-time images of tissue morphology. OCT can be used to study high-risk tissue sites without performing unnecessary biopsies and tissue removal.[32] Our group has shown that micro-invasive carcinoma can be distinguished from normal bronchial epithelium using epithelium thickness information measured by OCT. Also, AF bronchoscopy-guided OCT imaging of bronchial lesions is technically feasible.[33]

We hypothesize that an adjunctive optical technique, such as OCT, that provides complementary information to enable the rejection of AF false positives due to epithelial scattering may improve the specificity of AF bronchoscopy. Typical AF imaging systems measure the AF intensity at the tissue surface that includes epithelial scattering and absorption effects. Correcting AF intensity to remove the effect of absorption and scattering introduced by varying thicknesses of epithelium can identify the contribution of submucosa fluorophores to the AF signal. OCT can measure epithelium thickness directly and determine which portion of the AF signal loss to attribute to the additional epithelial scattering, as opposed to indicate a generalized fluorescence loss which may be due to collagen remodeling (potential precancer) or epithelial thickening. Information from OCT imaging, like the epithelium thickness and the backscattering coefficient within the epithelium, can be used to derive an AF correction factor. Therefore, given the structural information provided by OCT, a combined AF-OCT imaging system could have improved specificity compared with AF imaging alone.

In this work, we propose using coregistered AF-OCT imaging to model the effects of AF by the scattering and absorption properties of the epithelial layer. We use a two-layer tissue model in which the epithelium is the top layer and the stroma is the fluorescing bottom layer. The AF signal is assumed to be generated by fluorophores in the stroma alone. The two-layer tissue model is composed of a three-dimensional (3-D) tissue culture as the scattering layer (epithelium) fixed to a fluorescence slide as a uniformly fluorescing substrate (stroma). Experimental results from a bench-top AF-OCT imaging system and the two-layer tissue model are presented. The tissue cultures are grown from three different 3-D tissue cell cultures, namely HCT116, OVCAR8, and MCF7. The 3-D cell cultures are more similar to *in vivo* epithelium than other tissue phantoms (e.g., Intralipids and polystyrene sphere suspensions) in terms of biochemical and structural properties and are, therefore, more likely to have optical properties similar to *in vivo* epithelium. The OCT signal can be used to correct for the AF signal loss due to inflammation and epithelial thickening with the potential to reduce the resulting AF false positives.

2 Materials and Methods

2.1 *AF-OCT Imaging System*

Coregistered AF-OCT images were acquired using a custom bench-top dual-modality imaging system. The OCT subsystem included a 30-mW polygon-scanner-based wavelength-swept laser source with 106.8-nm bandwidth centered at 1321.4 nm with 40-kHz repetition frequency.[34] This laser source fed a fiber-based Mach–Zehnder interferometer (MZI) with reference and sample arms, as shown in Fig. 1 (OCT part). Another MZI unit was used at the source to generate the reference clock for sampling. The interference was detected by a balanced photodetector (PDB420A, ThorLabs, Newton, New Jersey) whose output was fed into a digitizer card (ATS460, AlazarTech, Pointe-Claire, Quebec) for signal processing and creating OCT images. The OCT subsystem provided images with about 8-μm axial and 20-μm lateral resolutions (in air).

The AF imaging subsystem used a 446 nm 40-mW semiconductor laser (CUBE 445-40C, Coherent, Santa Clara, California) as the excitation source. Two lenses (NA = 0.3) were used to collect the AF onto an APD-based detector (C5460, Hamamatsu, Japan). A dichroic filter separated backscattered blue light from AF photons as shown in Fig. 1 (AF part). The OCT and AF light beams were combined and separated by a backside-polished broadband dielectric mirror (BB1-E02P, ThorLabs) in free space. A Galvo-scanning mirror (GVS002, ThorLabs) provided a two-dimensional raster scan of both the AF and OCT beams on the sample. The AF and OCT channels were recorded simultaneously on the same high-speed digitizer ensuring their coregistration.

2.2 *Tissue Model*

The tissue model consisted of a 3-D cell culture grown on a membrane in a glass chamber mounted on a fluorescent slide, as shown in Fig. 2. The 3-D cell layer modeled the epithelium layer, while the fluorescent slide modeled the stroma. Three types of carcinoma cell lines were tested in the tissue model: HCT116 colorectal carcinoma, OVCAR8 ovarian carcinoma, and MCF7 breast adenocarcinoma.

2.3 *Cell Culture Materials and Methods*

2.3.1 *Cell Cultures*

MCF7 breast adenocarcinoma and HCT116 colorectal carcinoma cells were obtained from the American Type Culture Collection (Manassas, Virginia). OVCAR8 ovarian carcinoma cells were obtained from the NCI-Frederick Cancer DCTD Tumour/Cell Line Repository (Courtesy of Dr. Kevin Bennewith, BC Cancer Agency). OVCAR8 and HCT116 monolayer cell cultures were maintained in RPMI (Life Technologies, Carlsbad, California) and MCF7 in Dulbecco's minimal essential medium (Life Technologies). All cultures were supplemented with Glutamine (GlutaMax, Life Technologies) and 10% fetal bovine serum (Hyclone, Thermoscientific, Waltham, Massachusetts) and were incubated at 37°C, 95% air, and 5% CO_2.

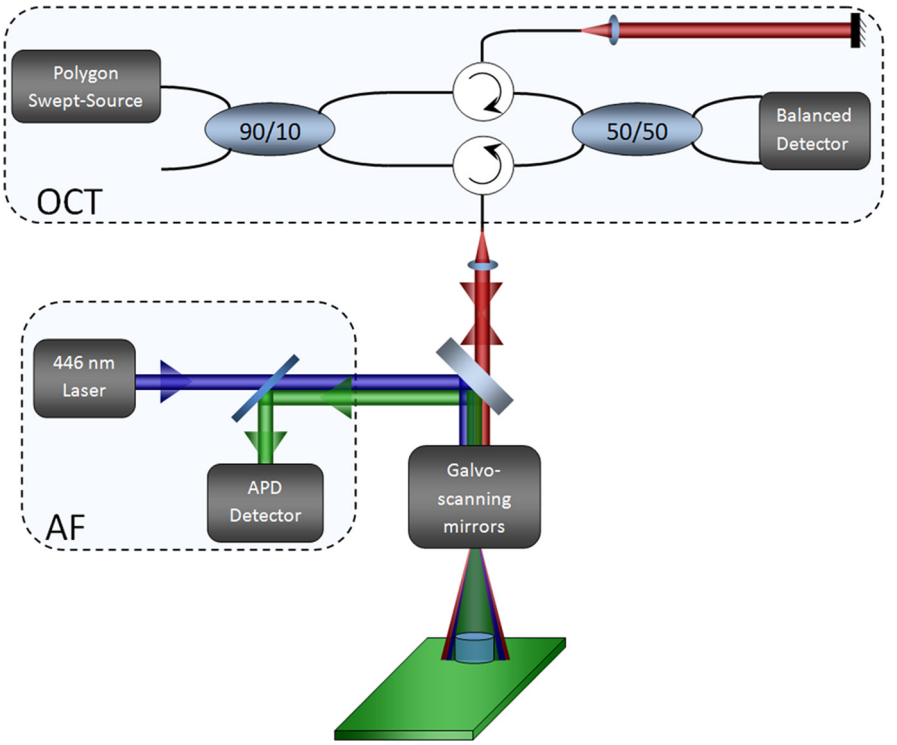

Fig. 1 Autofluorescence–optical coherence tomography (AF-OCT) imaging system.

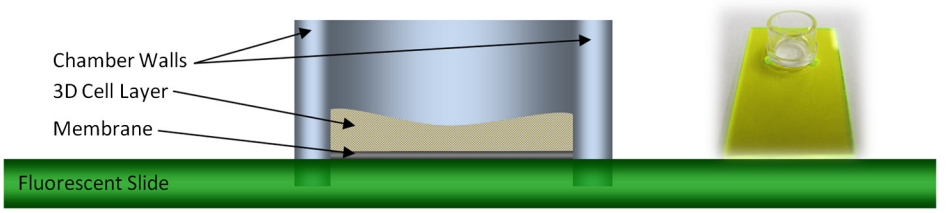

Fig. 2 Tissue model including a three-dimensional (3-D) carcinoma cell culture layer on a membrane in a glass chamber mounted on a fluorescent slide.

2.3.2 *3-D Tissue Disk Culture*

One hundred fifty microliters of 0.75 mg/mL collagen (bovine collagen type I, BD, Bedford, Massachusetts) was placed on the surface of the tissue culture insert membrane (Millicell CM 0.4 μm 12-mm tissue culture inserts, Millipore, Billerica, Massachusetts) and allowed to dry for 3 h before cells were plated. Approximately 1×10^6 cells were suspended in 0.5 mL media supplemented with penicillin and streptomycin (Life Technologies) and placed in the collagen-coated standing disks. The cells were allowed to settle on the porous membrane overnight in a 37°C tissue culture incubator, then transferred and suspended on a Teflon frame submerged in stirred media, and continuously gassed in 5% O_2, 5% CO_2, and balance N_2.[35,36]

2.4 *AF-OCT Imaging*

AF-OCT imaging was performed on the three different 3-D cell cultures, OVCAR8, HCT116, and MCF7, to obtain AF signal loss versus the cell layer thickness measured by OCT imaging. The 3-D cell cultures were established for 12 HCT116 samples, 16 OVCAR8 samples, and 14 MCF7 samples in an incubator. AF-OCT imaging was carried out over 6 days on the HCT116 samples (measured on days 1 to 6), over a 10-day period on OVCAR8 (measured on days 1, 2, 3, 4, 5, 6, 7, and 10), and over a 15-day period on MCF7 samples (measured on days 1, 2, 3, 5, 7, 12, and 15). Two samples were removed from the incubator on each imaging day, imaged using the bench-top AF-OCT system, and then either frozen for subsequent histology or discarded.

The 3-D cell layer thickness was measured directly from OCT images assuming the refractive index of the tissue culture to be 1.36.[37–41] AF signals were acquired simultaneously, providing information on the effects of different cell layer thicknesses. The measured AF signals were normalized to the reference signal obtained from imaging the chamber without the cell layer mounted on the fluorescent slide. The OCT images provided the cell layer ("epithelial") thickness, while the AF images provided the AF signal loss associated with the optical scattering and absorption of that layer.

2.5 *3-D Tissue Culture Histology*

Following AF-OCT imaging, the 3-D tissue disk cultures of days 3 and 6 for HCT116, days 3 and 10 for OVCAR8, and days 7 and

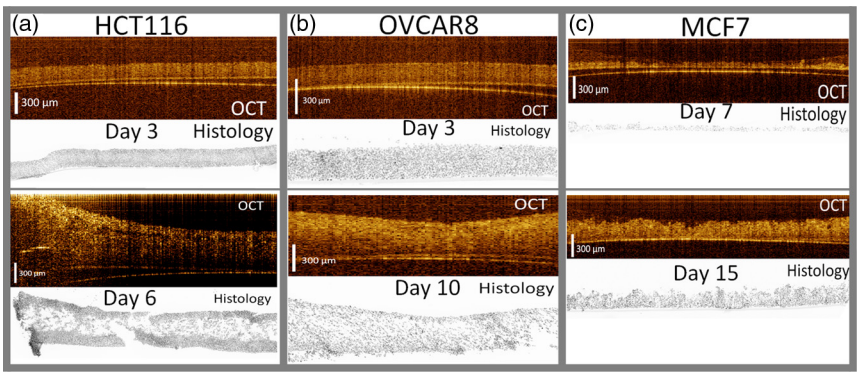

Fig. 3 OCT and stained fluorescence imaging (histology) of 3-D cell cultures of days 3 and 6 for HCT116 (a), days 3 and 10 for OVCAR8 (b), and days 7 and 15 for MCF7 (c).

15 for MCF7 were frozen in O.C.T. compound (TissueTek, Torrance, California) and stored at −20°C until sectioned. Using a cryostat, 10-μm sections were prepared and placed on positively charged glass slides. The cell nuclei were stained with 10 μM Hoechst 33342 (Sigma-Aldrich, St. Louis, Missouri) for 60 min to visualize the density of the tissue disks. Fluorescent images were acquired using a Brightline Pinkel filter set, Part Number DA/FI/TR/Cy5/Cy7-5X-A-000 (Semrock, Inc., Rochester, New York). The imaging system consisted of a robotic fluorescence microscope (Zeiss Imager Z1, Baden-Wurttenberg, Germany), a cooled monochrome CCD camera (Retiga 4000R; Q Imaging), a motorized slide loader, a translational x-y stage (Ludl Electronic Products, Hawthorne, New York), and customized ImageJ software running on a Macintosh computer.[36] Images were captured with 1.5-μm/pixel resolution. Imaging of these samples provides information for a thin sample and a thick sample for each 3-D cell culture type.

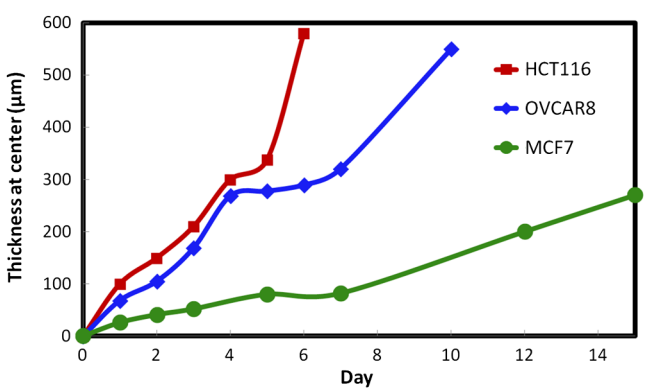

Fig. 4 3-D cell layer thickness at each imaging day post growth for HCT116 (red squares), OVCAR8 (blue diamonds), and MCF7 (green circles).

3 Results and Discussion

OCT images (top) and corresponding histology (bottom) for the three cell lines at two time points are shown in Fig. 3. The HCT116 and OVCAR8 3-D cell cultures maintain a more uniform layer structure with a smooth top surface compared with that of the MCF7 3-D culture. The thinner cultures appear more uniform, while the thicker cultures seem to have necrotic areas in the middle of the culture (far from nutrient sources during growth). Figure 4 shows the thickness at the center (averaged over 50 OCT A-lines or about 1 mm) of 3-D cell cultures corresponding to each imaging day after start of culture for HCT116 (red squares), OVCAR8 (blue diamonds), and MCF7 (green circles). HCT116 has the highest growth rate, and MCF7 has the lowest.

Two experiments were performed to verify that the measured fluorescence signal originated from the fluorescence slide and not from the cells or the cell-culture membrane. First, an empty chamber mounted half on the fluorescent slide and half on a glass slide [Fig. 5(a)] was imaged to measure the membrane fluorescence signal compared with the fluorescent slide signal. The results [blue curve in Fig. 5(a)] demonstrated that the membrane fluorescence signal is two orders of magnitude smaller than that of the slide. In the second experiment, the AF signal measured from a 3-D cell culture mounted on a fluorescent slide [Fig. 5(b)] was compared with that acquired when the 3-D cell culture was mounted on a glass slide [Fig. 5(c)]. The results showed that the fluorescence signal from the cells contributed up to only 2% of the total fluorescence signal.

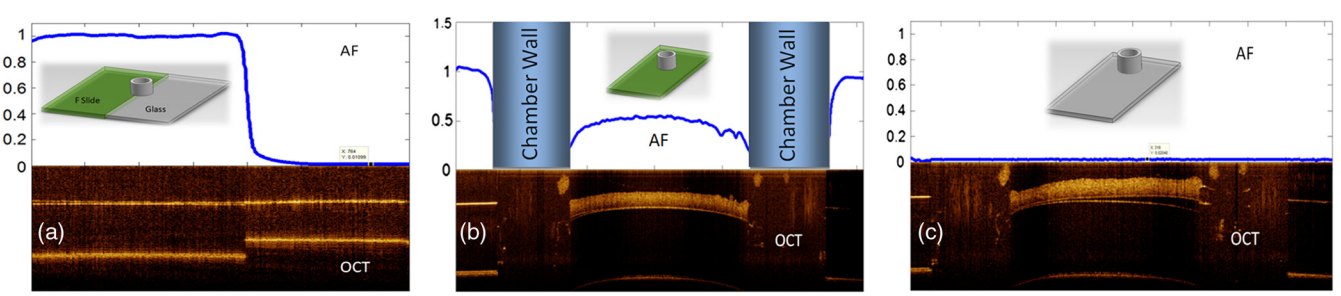

Fig. 5 (a) AF-OCT imaging of an empty chamber mounted half on the fluorescent slide and half on a glass slide, (b) AF-OCT imaging of the chamber with cells on the fluorescent slide, and (c) AF-OCT imaging of the chamber with cells on the glass slide.

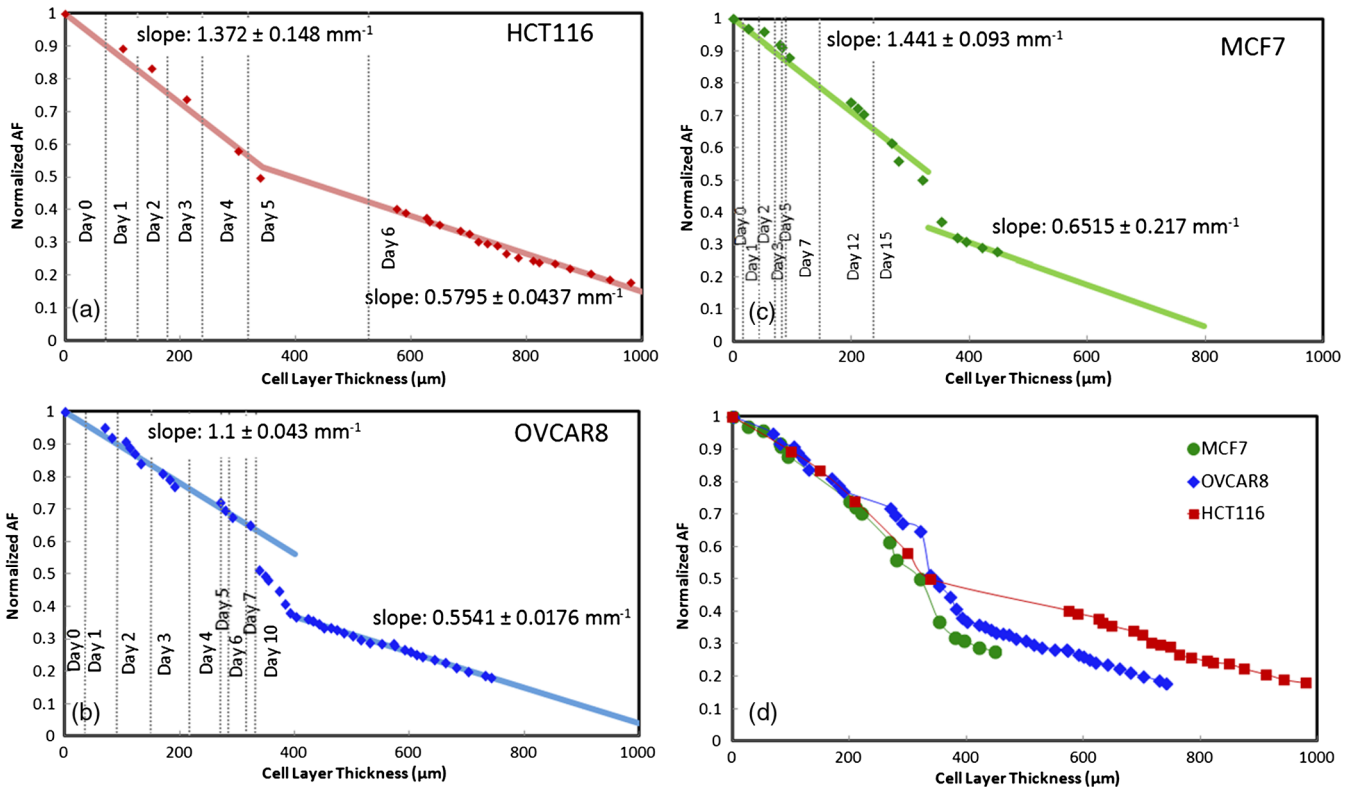

Fig. 6 AF loss versus 3-D cell layer thickness for HCT116 (a), OVCAR8 (b), and MCF7 (c) with piecewise linear fits. (d) Normalized AF data for three cell line types.

Therefore, the fluorescence signals from the cells and from the cell-culture membrane were assumed to be negligible compared with the fluorescent slide signal. Thus, we assume that the measured fluorescence signal in our 3-D model is only modified by the absorption and scattering properties of the cells, and there is no AF signal being added by the cells.

Figure 6 shows the normalized AF signal versus the 3-D cell layer thickness for HCT116 [Fig. 6(a)], OVCAR8 [Fig. 6(b)], and MCF7 [Fig. 6(c)] cells. For HCT116 and OVCAR8 cells, data were obtained for 6 and 7 consecutive days after start of culture, respectively, plus at day 10 for the OVCAR8 cultures. However, due to the very slow growth rate of MCF7, AF-OCT imaging measurements were set at larger intervals for the MCF7 case. OCT images showed relatively constant cell layer thicknesses along the lateral scan for thin layers, resulting in very few depth data points corresponding to each imaging day. However, the cell layer thickness changed significantly along the lateral scan in the OCT images of the later days, providing several data points for these thickness ranges.

For thin layers (<300 μm), the AF signal decreases approximately linearly with the cell layer thickness. The AF loss profile changes at some thickness point (in the 300 to 400 μm range) after which the AF loss decreases with a smaller linear fit slope compared with the thin layer profile for each cell line. For thick layers (>400 μm), the linear fit slopes are similar for the HCT116, OVCAR8, and MCF7 cell cultures albeit with different intercepts. The linear fit slopes are listed in Table 1.

The piecewise linear model illustrated in Fig. 6 was a better fit to the data than an exponential model (as indicated by the goodness of fit R^2). In the analytical model reported by Wu et al.,[42] AF signal loss is approximated by an exponential function with respect to the depth. However, the models presented by Li et al.[43] and Fantini and Gratton[44] suggest that the AF loss can be approximated to a linear function provided the optical properties at excitation and emission wavelengths are close.

We speculate that the change in the AF attenuation slopes for different thickness ranges can be attributed to the change in the 3-D cell layer morphology with respect to the thickness range. Comparing histology and OCT images of thin and thick 3-D cell cultures shown in Fig. 3, one can see that the thin 3-D cell cultures are fairly uniform. However, as the cell cultures grow thicker, there is apparent necrotic tissue and cell layer breakup in the mid-region. In the 3-D cell culture tissue, cells compete for oxygen and other nutrients. As explained extensively in Ref. 45, since the diffusion of oxygen is relatively low and oxygen consumption is high, diffusion can support only a limited

Table 1 Slopes of linear function fit (mm^{-1}) of autofluorescence (AF) attenuation for thin (<300 μm) and thick (<400 μm) 3-D cell layers for the HCT116, OVCAR8, and MCF7 cell cultures along with optical coherence tomography (OCT) A-line decay coefficients.

	HCT116	OVCAR8	MCF7
Slopes for layers <300 μm	1.372 ± 0.148	1.1 ± 0.043	1.441 ± 0.093
Slopes for layers <400 μm	0.579 ± 0.0437	0.554 ± 0.0176	0.651 ± 0.217
OCT A-line decay coefficient	2.366	6.765	8.633

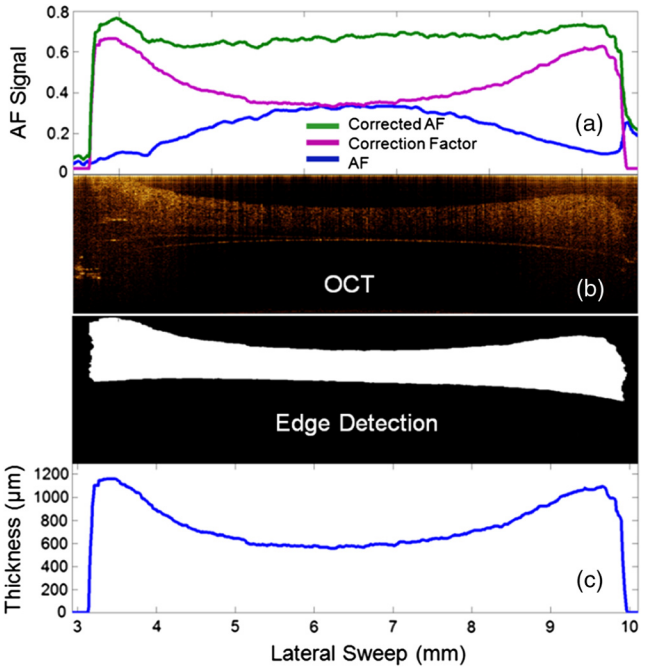

Fig. 7 (a) AF signal (blue curve), correction factor (purple curve), and corrected AF (green curve), along the lateral sweep, (b) OCT image, (c) edge-detected image, and (d) cell layer thickness obtained from edge detection.

number of cells before the balance between metabolic demand and diffusion creates a zone in the center where oxygen tension is too low to support viable cells, resulting in central necrosis. In Ref. 45, the authors estimated that few cells tolerate diffusion distances >0.2 mm. We postulate that these necrotic tissue regions (with spatially varying cell densities) decrease optical absorption and scattering of the cell culture in this region, leading to a smaller AF attenuation slope. The empty regions cannot scatter or absorb photons. A natural implication is that the existence of these empty regions makes the absorption and scattering loss effects less severe versus the depth compared with the case where these regions are filled out with scattering and absorbing particles.

As illustrated in Fig. 6(d), the data suggest that for small thicknesses (<300 μm), the cells behave very similarly in terms of AF loss with the average decrease rate of 1.3 mm^{-1}. This thickness range is particularly important, since the lung epithelium layer thickness lies typically in this range. We propose that results from this epithelial tissue model can be used to correct for AF *in vivo* attenuation by the lung epithelial layer. Removing AF variation due to epithelial scattering could potentially reduce AF false positives due to inflammation and epithelial thickening. For thicker layers, however, the data show that the AF scattering loss is very different for different cell line types; for a fixed thickness, HCT116 shows the least AF scattering loss, MCF7 shows the most, and OVCAR8 loss is in between but closer to MCF7. However, the slopes of the fitted linear functions are also very close for the three cell lines with the average slope of 0.59 mm^{-1}, even though the offsets are quite different. Therefore, the AF signal loss can be estimated relative to one data point corresponding to a specific thickness using this relatively constant slope. In addition, the lack of cellular homogeneity observed in the thick 3-D cultures may not occur as frequently in *in vivo* tissue, and the thick *in vivo* case may be more similar to the thin 3-D culture cases.

The measured AF signal may be affected by geometrical factors such as the tissue model–lens distance that can be measured using the technique reported in Ref. 46. To minimize these effects, the experimental results are normalized to the reference

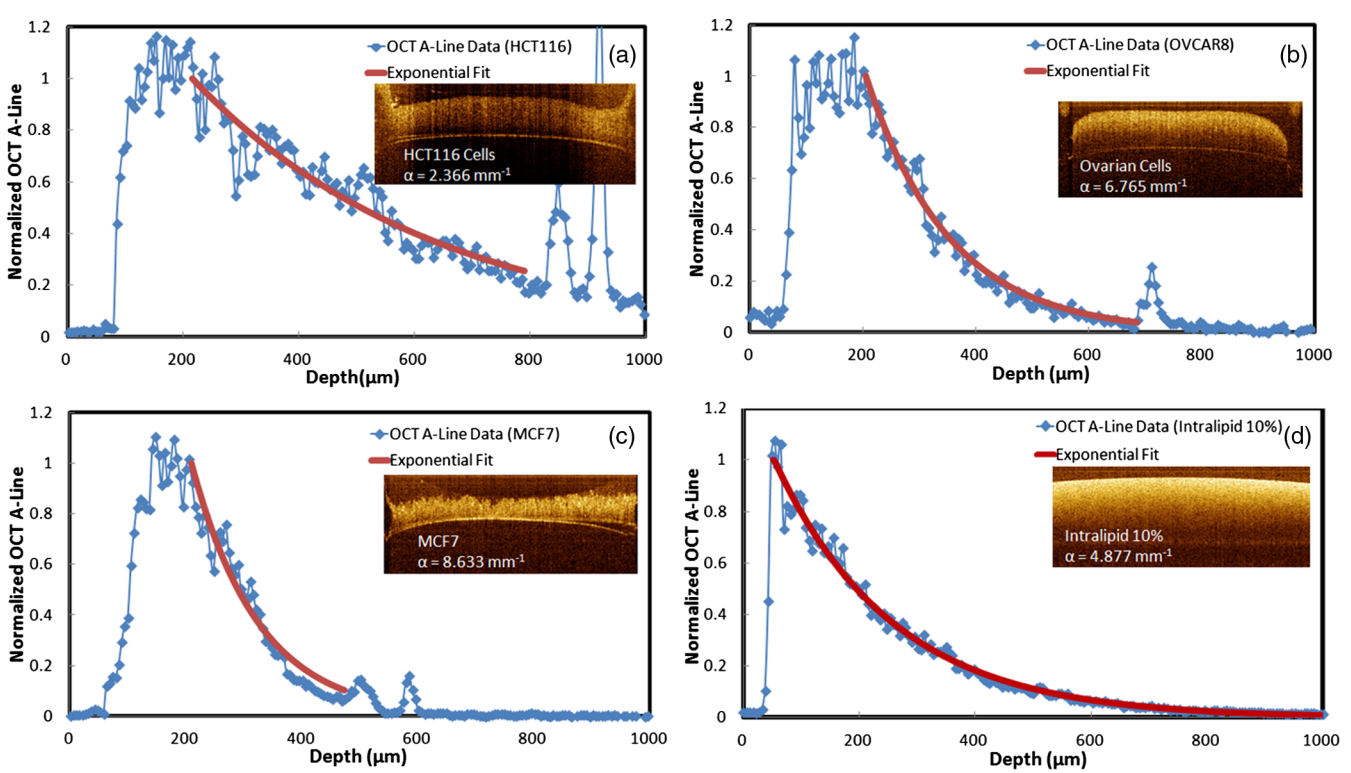

Fig. 8 Normalized OCT A-line data and corresponding exponential fits for HCT116 (a), OVCAR8 (b), MCF7 (c), and Intralipid 10% (d).

signal obtained from imaging the chamber without the cell layer mounted on the fluorescent slide. The normalization cancels out the factors that linearly change the AF intensity and mitigates higher-order effects. In *in vivo* cases, where there is no reference signal to which the AF signal can be normalized, the method reported in Ref. 46 can be used.

We applied the proposed AF correction method on the tissue model data shown in Fig. 7(b), in which the cell layer thickness varies across the lateral scan direction. The AF signal [blue curve in Fig. 7(a)] is also varying with respect to the layer thickness. Illustrated in Fig. 7(d) is the cell layer thickness obtained by applying edge detection to the OCT image using the Magnetic Lasso tool of Photoshop [Fig. 7(c)]. The correction factor, shown in purple in Fig. 7(a), was calculated using the layer thickness, AF signal at the center, and the average (across the three tissue types) AF loss slope (0.59 mm^{-1}) obtained from the culture data. The correction results in much more constant AF signal [shown in green in Fig. 7(a)] regardless of the cell layer thickness variations.

Figure 8 shows the OCT A-line data obtained from the final days of imaging for the HCT116, OVCAR8, and MCF7 3-D cultures. Curve-fitting of an exponential function to the A-line data results in the OCT backscattering coefficients listed in Table 1. The A-line decay coefficients are consistent with AF loss for thick cell layer with the highest loss for MCF7 and the lowest for HCT116. Also, comparison of the shapes of A-line data for the 3-D cell cultures and for Intralipid reveals the nonuniformity of the cells density compared with a homogenous medium like Intralipid. We expect that the cell lines are closer models of *in vivo* tissue layers than Intralipids in terms of biochemical and structural properties.

The results presented from the 3-D cell culture model will likely be different from those one would observe *in vivo* from real bronchial mucosa. The underlying correction principle, however, is still applicable to *in vivo* imaging and will provide the clinician with additional information that may eventually improve the specificity in the identification of intraepithelial neoplastic lesions. Additional *in vivo* studies, on surrogate epithelial tissues or in an animal model, are required to validate the piecewise linear model and to derive a clinically relevant method for correction of the AF signal.

4 Conclusion

There are many structural and molecular changes associated with neoplastic epithelial development in the bronchial passages of the lung. Many of these changes are manifest in the underlying submucosa as well as in the epithelium itself. Removing the effects of optical scattering and absorption associated with the overlying epithelial layer from the AF signal generated by the submucosa and underlying structures can improve the measurement of the relative contribution of fluorophores and structural changes associated with neoplasia in the submucosa *in situ*. We proposed using coregistered AF-OCT imaging to measure the magnitude and spatial variation of scattering and absorption by the epithelium and to correct the AF signal using this information. The thickness of the epithelial layer can be directly measured by OCT imaging, while AF imaging records a signal convolved with AF signal loss due to scattering and absorption by this epithelial layer. The AF loss measured from AF-OCT imaging of different 3-D carcinoma cell cultures (HCT116, OVCAR8, and MCF7) is presented in this work. The data suggest that for thin cell layers (<300 μm), different cell lines behave very similarly in terms of amount of AF loss generated, with an average linear attenuation of 1.3 mm^{-1}. Given this attenuation rate, the absolute value of AF modification can be estimated for this thickness range. For thicker layers (>400 μm), AF loss appears quite different for the different cell lines. However, the slope of AF loss is relatively constant, with the average of 0.59 mm^{-1}. Therefore, the AF loss can be predicted relative to one known data point given this relatively constant slope. The data presented here can be used to correct for AF signal loss due to scattering and absorption of epithelium and potentially to rule out false positives due to inflammation and epithelial thickening.

Acknowledgments

This work was supported by funding from the Michael Smith Foundation for Health Research (MSFHR) and Lotte & John Hecht Memorial Foundation.

References

1. World Health Organization Fact sheet N°297, http://www.who.int/mediacentre/factsheets/fs297/en/ (February 2013).
2. S. Lam, "Detection of preneoplastic lesions," Chapter 6 in *Lung Cancer*, J. A. Roth et al., Eds., 3rd ed., Blackwell Scientific Publications, Boston (2007).
3. S. Lam et al., "The role of autofluorescence bronchoscopy in diagnosis of early lung cancer," in *IASLC Textbook of Prevention and Detection of Early Lung Cancer*, F. R. Hirsch et al., Eds., pp. 149–160, Taylor & Francis, New York (2005).
4. P. Parsa, S. L. Jacques, and N. S. Nishioka, "Optical properties of rat liver between 350 and 2200 nm," *Appl. Opt.* **28**(12), 2325–1330 (1989).
5. M. Xu and R. R. Alfano, "Fractal mechanisms of light scattering in biological tissue and cells," *Opt. Lett.* **30**(22), 3051–3053 (2005).
6. J. R. Mourant et al., "Mechanisms of light scattering from biological cells relevant to noninvasive optical-tissue diagnostics," *Appl. Opt.* **37**(16), 3586–3593 (1998).
7. P. Lee, W. Gao, and X. Zhang, "Performing of single-scattering model versus multiple-scattering model in the determination of optical properties of biological tissue with optical coherence tomography," *Appl. Opt.* **49**(18), 3538–3544 (2010).
8. J. M. Schmitt, A. Knuttel, and R. F. Bonner, "Measurement of optical properties of biological tissues by low-coherence reflectrometry," *Appl. Opt.* **32**(30), 6032–6042 (1993).
9. S. L. Jacques, B. Wang, and R. Samathan, "Reflectance confocal microscopy of optical phantoms," *Biomed. Opt. Express* **3**(6), 1162–1172 (2012).
10. R. S. Bradley and M. S. Thorniley, "A review of attenuation correction techniques for tissue fluorescence," *J. R. Soc. Interface* **3**(6), 1–13 (2006).
11. F. F. Jöbsis et al., "Intracellular redox change in functioning cerebral cortex. I. Metabolic effects of epileptiform activity," *J. Neurophysiol.* **34**(5), 735–749 (1971).
12. H. Franke, C. H. Barlow, and B. Chance, "Oxygen delivery in perfused rat kidney: NADH fluorescence and renal functional state," *Am. J. Physiol.* **231**(4), 1082–1089 (1976).
13. K. Harbig et al., "In vivo measurement of pyridine nucleotide fluorescence from cat brain cortes," *J. Appl. Physiol.* **41**(4), 480–488 (1976).
14. A. Mayevsky and B. Chance, "Intracellular oxidation-reduction state measured in situ by a multichannel fiber-optic surface fluorimeter," *Science* **217**(4559), 537–540 (1982).
15. R. S. Kramer and R. D. Pearlstein, "Cerebral cortical microfluorometry at isosbestic wavelengths for correction of vascular artefact," *Science* **205**(4407), 693–696 (1979).
16. H. J. C. M. Sterenborg et al., "Evaluation of spectral correction techniques for fluorescence measurements on pigmented lesions in vivo," *J. Photochem. Photobiol. B* **35**(3), 159–165 (1996).
17. B. Pogue and T. Hasan, "Fluorophore quantitation in tissue-simulating media with confocal detection," *IEEE J. Sel. Top. Quant. Electron.* **2**(4), 959–964 (1996).

18. B. W. Pogue and G. Burke, "Fiber-optic bundle design for quantitative fluorescence measurement from tissue," *Appl. Opt.* **37**(31), 7429–7436 (1998).
19. K. R. Diamond, T. J. Farrell, and M. S. Patterson, "Measurement of fluorophore concentrations and fluorescence quantum yield in tissue-simulating phantoms using three diffusion models of steady-state spatially resolved fluorescence," *Phys. Med. Biol.* **48**(24), 4135–4150 (2003).
20. K. R. Diamond, M. S. Patterson, and T. J. Farell, "Quantification of fluorophore concentration in tissue-simulating media by fluorescence measurements with a single optical fiber," *Appl. Opt.* **42**(13), 2436–2442 (2003).
21. N. C. Biswal et al., "Recovery of turbidity free fluorescence from measured fluorescence: an experimental approach," *Opt. Express* **11**(24), 3320–3331 (2003).
22. R. Richards-Kortum et al., "A one-layer model of laser-induced fluorescence for diagnosis of disease in human tissue: applications to atherosclerosis," *IEEE Trans. Biomed. Eng.* **36**(12), 1222–1232 (1989).
23. W. Lin et al., "Intraoperative application of optical spectroscopy in the presence of blood," *IEEE J. Sel. Top. Quant. Electron.* **7**(6), 996–1003 (2001).
24. A. J. Durkin et al., "Relation between fluorescence spectra of dilute and turbid smaples," *Appl. Opt.* **33**(3), 414–423 (1994).
25. X. D. Li et al., "Fluorescent diffuse photon density waves in homogeneous and heterogeneous turbid media: analytic solutions and applications," *Appl. Opt.* **35**(19), 3746–3758 (1996).
26. N. N. Zhadin and R. R. Alfano, "Correction of the internal absorption effect in fluorescence emission and excitation spectra from absorbing and highly scattering media: theory and experiment," *J. Biomed. Opt.* **3**(2), 171–186 (1998).
27. D. Stasic, T. J. Farrell, and M. S. Patterson, "The use of spatially resolved fluorescence and reflectance to determine interface depth in layered fluorophore distributions," *Phys. Med. Biol.* **48**(21), 3459–3474 (2003).
28. A. J. Durkin, D. L. Farkas, and A. P. Koretsky, "Calcium measurements in perfused mouse heart: quantitating fluorescence and absorbance of rhod-2 by application of photon migration theory," *Biophys. J.* **80**(1), 549–561 (2001).
29. D. Huang et al., "Optical coherence tomography," *Science* **254**(5035), 1178–1181 (1991).
30. J. G. Fujimoto et al., "Optical biopsy and imaging using optical coherence tomography," *Nat. Med.* **1**(9), 970–972 (1995).
31. G. J. Tearney et al., "In vivo endoscopic optical biopsy with optical coherence tomography," *Science* **276**(5321), 2037–2039 (1997).
32. M. Tsuboi et al., "Optical coherence tomography in the diagnosis of bronchial lesions," *Lung Cancer* **49**(3), 387–394 (2005).
33. S. Lam et al., "In vivo optical coherence tomography imaging of preinvasive bronchial lesions," *Clin. Cancer Res.* **14**(7), 2006–2011 (2008).
34. S. H. Yun et al., "High-speed wavelength-swept semiconductor laser with a polygon-scanner-based wavelength filter," *Opt. Lett.* **28**(20), 1981–1983 (2003).
35. A. H. Kyle et al., "Direct assessment of drug penetration into tissue using a novel application of three-dimensional cell culture," *Cancer Res.* **64**(17), 6304–6309 (2004).
36. A. H. Kyle, J. H. Baker, and A. I. Minchinton, "Targeting quiescent tumor cells via oxygen and IGF-I supplementation," *Cancer Res.* **72**(3), 801–809 (2012).
37. C. L. Curl et al., "Refractive index measurement in viable cells using quantitative phase-amplitude microscopy and confocal microscopy," *Cytometry A* **65**(1), 88–92 (2005).
38. J. Y. Lee et al., "Single live cell refractometer using nanoparticle coated fiber tip," *Appl. Phys. Lett.* **93**(17), 173110 (2008).
39. F. Lanni, A. S. Waggoner, and D. L. Taylor, "Structural organization of interphase 3T3 fibroblasts studied by total internal reflection fluorescence microscopy," *J. Cell Biol.* **100**(4), 1091–1102 (1985).
40. W. J. Choi et al., "Full-field optical coherence microscopy for identifying live cancer cells by quantitative measurement of refractive index distribution," *Opt. Express* **18**(22), 23285–23295 (2010).
41. H. Ding et al., "Determination of refractive indices of porcine skin tissues and Intralipid at eight wavelengths between 325 and 1557 nm," *J. Opt. Soc. Am. A* **22**(6), 1151–1157 (2005).
42. J. Wu, M. S. Feld, and R. P. Rava, "Analytical model for extracting intrinsic fluorescence in the turbid media," *Appl. Opt.* **32**(19), 3585–3595 (1993).
43. X. D. Li et al., "Fluorescent diffuse photon density waves in homogeneous and heterogeneous turbid media: analytic solutions and applications," *Appl. Opt.* **35**(19), 3746–3758 (1996).
44. F. Fantini and E. Gratton, "Fluorescence photon-density waves in optically diffusive media," *Opt. Commun.* **173**, 73–79 (2000).
45. G. F. Muschler, C. Nakamoto, and L. G. Griffith, "Engineering principles of clinical cell-based tissue engineering," *J. Bone Joint Surg. Am.* **66-A**(7), 1541–1558 (2004).
46. M. J. Booth and T. Wilson, "Refractive-index-mismatch induced aberrations in single-photon and two-photon microscopy and the use of aberration correction," *J. Biomed. Opt.* **6**(3), 266–272 (2001).